

**Land Surveying Division,
Hong Kong Institute of Surveyors**

Research Report 2021-2022

**Systematic review on the change detection of land use
and land cover over urbanized areas using very high-
resolution remote sensing images**

Prepared by :

Dr. Conrad Tang

Conrad Tang & Associates Limited

&

Prof. Charles Wong, Ms. Jing Li, Ms. Meilian Wang, Dr. Felix Zhu & Dr.

Guoqiang Shi

Department of Land Surveying and Geo-Informatics

The Hong Kong Polytechnic University

Systematic review on the change detection of land use and land cover over urbanized areas using very high-resolution remote sensing images

Abstract:

The change of the Earth's surface resulting from human activities, such as land reclamation has been studied for past decades. Particularly, research on land use and land cover (LULC) transformation is of great significance for exploring and understanding local and even regional land-use changes, which can serve as a scientific foundation for land use, town planning, and urban redevelopment. This study thus provides a systematic review on LULC change detection technology and applications for assisting the development based on the Hong Kong Smart City initiative and facilitating the implementation of the Common Spatial Data Infrastructure in Hong Kong.

Keywords: Remote sensing; Land use and land cover; Pixel-based change detection; Object-based change detection

Systematic review on the change detection of land use and land cover over urbanized areas using remote sensing images

1. Introduction

With the global urbanization and economic development during the last three decades, the earth's surface has experienced increasingly rapid and comprehensive changes, including changes in land use and land cover. Land use is referred to the land that people use it for, while land cover is referred to the features on the earth's surface (Mishra et al., 2017). This information is critical for natural resource management, ecosystem and biodiversity conservation, and decision support for sustainable development. Quantifying changes in Land Use and Land Cover (LULC) has significant consequences for planning, surveying, transportation, and the economy since urban areas are the centers of human activity (Chi Zhang et al., 2019). Singh stated that "change detection is the technique of identifying differences in an object's or phenomenon's status across time by monitoring it at various times" (Singh, 1989).

Remote sensing (RS) is a technique that acquires, extract, and analyze information about objects or phenomenon without physical connection (Campbell et al., 2011). It starts with a photograph of Paris from a balloon in 1958 (Rogan et al., 2004). Then the systematic development is carried by World War I and the climax development is reached during the Cold War (Wong et al., 2021). Its recent development is with the increase of small sensor pods (Campbell et al., 2011). Simultaneously, with the development of science and technology, the quality of data captured by RS is improved significantly, becoming an increased power and effective tool facilitating the synoptic analysis of pattern and dynamic changes of LULC at local, regional, and global scales over time and heightening awareness of the critical nature of assessing LULC changes for comprehending and interaction between individuals and the environment (Dewan et al., 2009; Onur et al., 2009; Reid et al., 2000). Particularly, retrospective and consistent synoptic coverage of satellite photographs provide depth insight into the area that has high-speed changes (Dewan et al., 2009).

RS data usually is in the form of multi- or hyper-resolution images. These RS images have been widely used in change detection since they span a broad geographic

area and are available in a wide variety of spatial, spectral, and temporal resolutions (Ban et al., 2016a). For example, X. Chen et al. (2005) used Landsat 4 and Landsat 7 images to analyze the landscape change of Siberian city between 1990, 2000, and 2001. Wang et al. (2022) evaluated the land use cover changes of Nanjing, Xianning, and Zhejiang in 2016, 2017, 2019, and 2021 using SPOT 7, Sentinel-2, and Landsat 8 images. In addition, some change detection techniques use remote sensing images with a combination of Geographic Information System (GIS) technique which can incorporate multisource datasets for change detection (Alqurashi et al., 2013). RS and GIS datasets were integrated by Brondizio et al. (1994) to assess the patterns of land use changes in the Amazon forest based on Landsat TM scenes from 1985 to 1991. This combined technique is also extensively applied in a variety of sectors, including the studies of urbanization (Ban et al., 2012; Taubenböck et al., 2012), deforestation (Achard et al., 2002; Desclée et al., 2006), desertification (Dawelbait et al., 2012; Yang et al., 2005), flooding, disaster monitoring (Martinez et al., 2007; Martinis et al., 2011), and glacier monitoring (Akbari et al., 2014).

A variety of change detection approaches and algorithms have been proposed and evaluated. These methods have been designed to target different components of the change detection process, which usually include speckle reduction in the context of change detection (O. Yousif et al., 2013), extraction of detailed 'from-to' change information using pre- and post-classification comparison (Alphan et al., 2009), spatial-contextual change detection (Osama Yousif et al., 2014), unsupervised change detection (Francesca Bovolo et al., 2006), feature-based and pixel-based change detection (Gamba et al., 2006), and object-based change detection (Bontemps et al., 2008; Desclée et al., 2006; Qin et al., 2013; Osama Yousif et al., 2015). However, the detection of changes using multitemporal remotely sensed images is complicated considering the uncertainties in the measured phenomenon, limitations in the imaging sensors' ability to measure ground changes, inherent noise in the imaging process, and uncertainties in the change detection process, as well as factors like phenology, soil moisture, and sun and satellite/platform viewing angles. There is no single solution that is capable of resolving all forms of change detection challenges. Different applications require different approaches, and very high resolution remote sensing images with enhanced spatial,

spectral, radiometric, and temporal resolution can be used to facilitate the new Smart City initiatives.

The project/review paper is aiming to review recent improvements in change detection approaches by employing multi-temporal remote sensing images. Specifically, a series of change detection techniques, including processing, algorithms, and accuracy assessment will be discussed. The pixel-based and object-based change detection will be elaborated. The primary change detection workflow is illustrated as follows in.

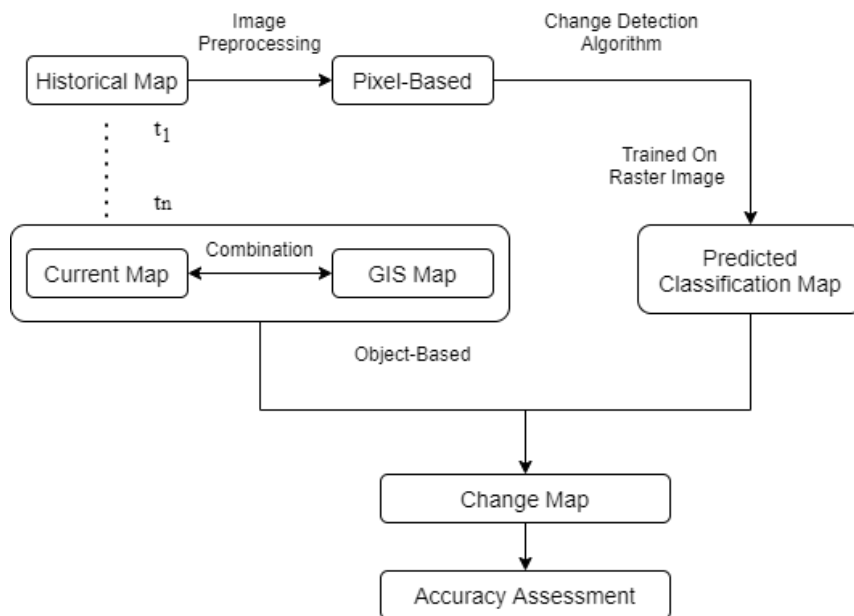


Figure 1. The primary LULC change detection workflow.

2. A review of land cover land use change detection methodologies

2.1. Pixel-based change detection

A pixel is a fundamental unit for image analyses and change detection approaches. For pixel-based change detection algorithms, a pixel of a digital image is the smallest unit whose spectral features will be used to identify and analyze changes without considering the environmental scope. RS images are used for change detection since any changes in LULC should be reflected by the differences in radiance/reflectance values. When compared to those produced by other variables, radiance/reflectance changes induced by LULC should be significant (Ingram et al., 1981). These determinants include variations in atmospheric conditions, changes in solar radiation, and variations in soil moisture

(Jensen, 1983). By incorporating with relevant ancillary data, the effects of the mentioned variables can be minimized.

2.1.1.1. Change detection by comparing bitemporal data

Change detection can be carried out by directly comparing data of two different dates in a pixel-by-pixel, thus, to highlight the changed areas. Numerous methods of this category mainly can be classified in terms of two aspects, i.e., the comparison strategy performed, and the data used for comparison. The algebraic operator of differencing and ratioing are two common strategies for comparison. The data used for comparison could be the original bands of reflectance, composited indices from original bands (e.g., the normalized difference vegetation index), and transformed features (e.g., principal components) from original bands. A schematic diagram of this category is displayed in Figure 2.

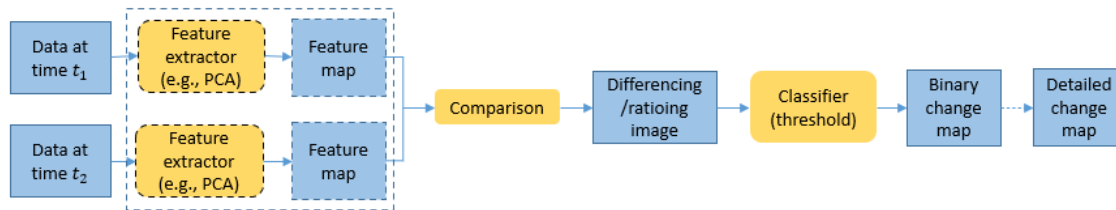


Figure 2. schematic diagram of change detection by comparing bitemporal data

2.1.1.1.1. Image differencing

The most extensively used approach for change detection is image differencing, which has been utilized in a number of geographical regions. This method assumes that a change in land use will generally lead to a change in land cover and a change in spectral radiances or reflectance of that land unit consequently (Quarmby et al., 1989).

It is a simple and straightforward method for detecting and interpreting changes (Weismiller et al., 1977). It categorizes image pixels as either changed or remain unchanged. These results are achieved by subtracting the digital number assigned to a pixel in the image taken at one time-stamp and extracting from that assigned pixel to the analogous pixel in the image taken at another time-stamp (Singh, 1989). A differencing image can be generated from two spatially registered images of time t_1 and t_2 in a pixel-to-pixel manner, which is formulated as:

$$Dx_{ij}^k = x_{ij}^k(t_2) - x_{ij}^k(t_1) + C$$

where x_{ij}^k is the pixel at row i , column j in the band k and C is a constant to produce positive digital numbers. The image differencing can be applied on original bands of image reflectance and it has also been used for differencing of mainly relevant vegetation indices constructed from multiple bands, such as the ratio vegetation index, normalized difference vegetation index, transformed vegetation index (Singh, 1989). Such change detection specifically on vegetation provide an avenue for deciding whether or not a vegetation canopy has been significantly altered (Nelson, 1983).

2.1.1.2. Image ratioing

Ratioing is thought to be a reasonably quick technique of detecting areas of change. Two registered images from different dates with one or more bands are ratioed correspondingly in a pixel-by-pixel basis, formulated as:

$$Rx_{ij}^k = \frac{x_{ij}^k(t_1)}{x_{ij}^k(t_2)}$$

The ratio of the pixel should be near or close to 1 if negligible changes occur and can deviate largely from 1 if considerable changes occur due to the change of the reflected energy. The ratio of two registered images from different dates containing one or more bands is computed band by band (Singh, 1989). It is used to emphasize tiny differences in the pixels of diverse land covers and can reduce the effect of shadows, radiation variation, image noise, and solar angle (Alphan, 2011a).

2.1.1.3. Feature transformation

Feature transformation can be performed in advance of comparison. It is a multivariate technique for lowering dataset dimensionality, which is used in remote sensing transformation (Singh et al., 1985). Principal Component Analysis (PCA) is a strategy for minimizing the quantity of spectrum and maximizing the variance of the major components (Singh, 1989). In multitemporal studies, for an example, the PCA method catenate the four-band Landsat scenes of the same area which are recorded at different dates, and such catenated bands can be treated as a single multiple-band data set, on which PCA analysis can be performed. This major component images generated should reveal the gross differences related with overall radiation and atmospheric changes and the minor components are associated with local changes in land cover (Richards, 1984).

It was claimed that incorporating standardized variables in the PCA improved the signal-to-noise ratio and image enhancement significantly (Singh et al., 1985). Besides, the tasseled cap transformation (TCT) has been widely and mainly used for vegetation change detection (Jin et al., 2005). The TCT is originally designed for the Landsat satellite by applying a linear transformation on its spectral bands to extract the physical indicators of brightness, greenness and wetness (Jin et al., 2005). The linear coefficients used for TCT is sensor specific and should be determined case by case.

Two critical components of the differencing, ratioing and feature transformation methods are the image registration and threshold selection. Robustness and strict image registration should be performed to avoid the pseudo-change caused by misregistration. To visualize the changes between images, it is critical to choose an appropriate ratioing threshold value. The choice of threshold is normally arbitrary in a trial-and-error process to achieve an optimal one. Rogerson (2002) offered a statistical framework for the selection of thresholds with special attention to global autocorrelation. From a visualization perspective, the methods for change detection by comparing bi-temporal data are mainly used to highlight changed areas effectively. Examples has been given in Figure 3 in which changed areas are highlighted with various combinations of bands constructed by differencing, ratioing and principal component. With the appropriate determined threshold, the image can be divided into binary change, i.e., changed or no-changed.

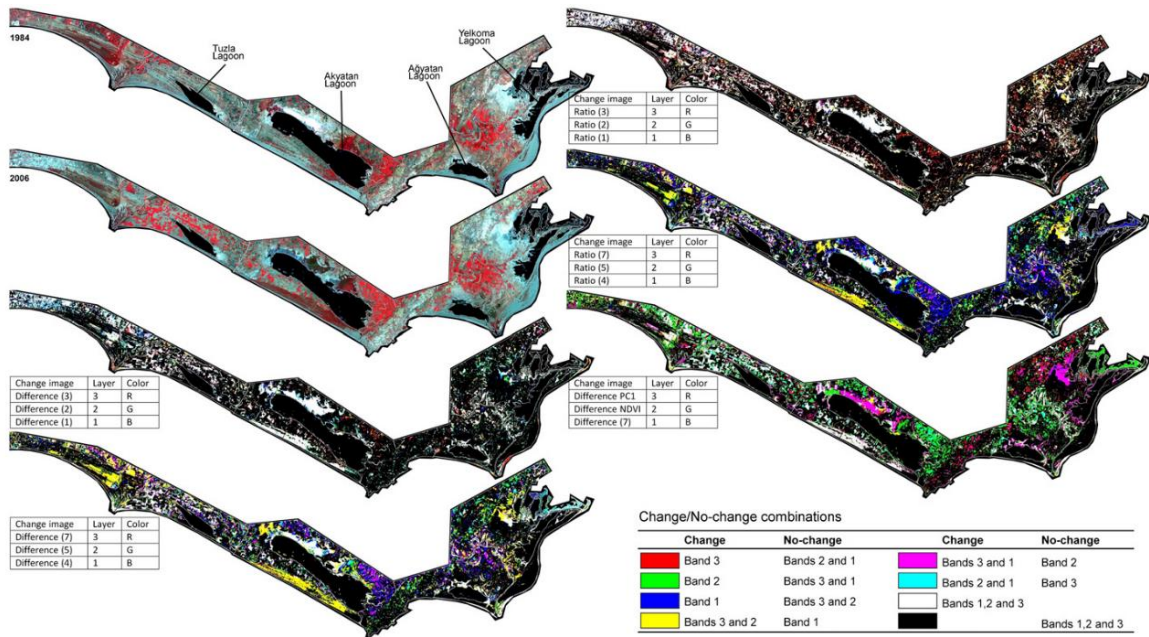


Figure 3. Spatial representation of changes as RGB composites of binary change images (cited from Alphan (2011b))

2.1.2. Change detection by stacking multi-date data

In addition to detect changes by comparing the data in two different dates, change detection can also be carried out by stacking or fusing data set spanning a certain period of time to directly identify the changed areas. A schematic diagram illustrating the category method is shown in Figure 4. For instance, the four visible to near-infrared bands of Landsat at two dates can be stacked to form an eight-band composited data and the analysis. Subsequent feature analysis and/or classification are applied on the composited data. The feature analysis can also be the PCA as that introduced in Section 2.1.1.3. Both supervised and unsupervised modes can be employed for classification. In the supervised mode, training sets (changed or unchanged areas) are utilized to identify the input space of the classifier in a supervised approach. In unsupervised mode, cluster analysis is used to classify scenes that have undergone known modifications (Singh, 1989).

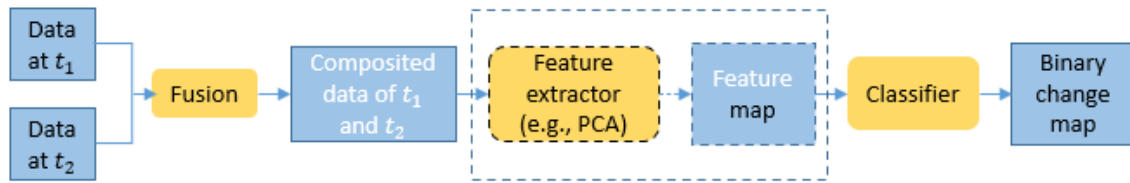


Figure 4. schematic diagram of change detection by stacking multi-date data

Although this approach only requires a single classification, it is a sophisticated method with numerous classes and features (temporal and spectral), among which redundancy can appear (Estes et al., 1982). Such redundancy problem can be partly overcome by adopting a PCA transformation on the original data set and major variance can be represented in the first few components that will be used in the subsequent classification procedure. Another challenge is that the temporal and spectral variables in the combined dataset have equal status (Schowengerdt, 2012), making it difficult to distinguish whether the changes are spectral or temporal in the classification result. Swain (1978) proposed a Bayesian classifier to partly eliminate this coupling effect

2.1.3. Change detection by post-classification

Post-classification comparison is an effective approach for change detection, which needs the comparison of separately categorized images. By properly coding the categorization outcomes of two different dates, the entire matrix of changes can be depicted. Additionally, due to the selective grouping of categorization results, any changing subgroup may be relevant. Figure 5 displays the schematic diagram of this category of methods.

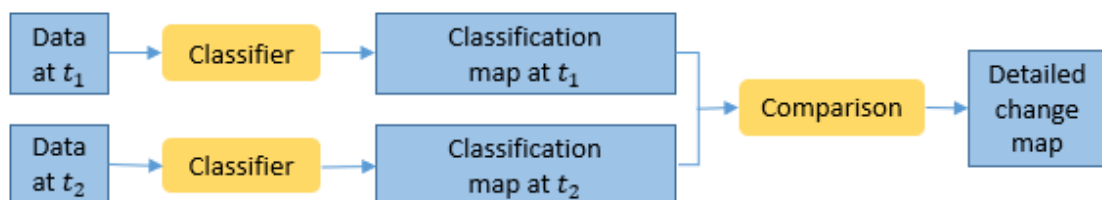


Figure 5. schematic diagram of change detection by post-classification

Post-classification comparisons are useful since they allow the separation of data from two dates, alleviating the issue of adjusting for atmospheric and sensor changes across dates (DA Stow et al., 1980). The solution also overcomes the issue of accurate registration of multiple-date images (Singh, 1989). However, an early study reveals significant mistakes in LULC change detection with Landsat images via post-classification method (Gordon, 1980) which was later evidenced by (Toll et al., 1981) that the low performance may be ascribed partly to the difficulty of obtaining similar classification results from images taken at different times. Individual image classification errors could be transmitted in the resulting map, leading to lower change detection accuracy (Lillesand et al., 2015). Individual image classification must be as precise as possible in order to optimize change detection outcomes.

2.2. Object-based change detection

While the abovementioned pixel-based approaches for change detection are conducted at a pixel-by-pixel, the object-based approaches are performed on object level. The term object is defined as a group of pixels with homogeneous spectral characteristics and continuous spatial distribution (Benz et al., 2004). A critical procedure in object-based change detection is to extract objects from images through segmentation strategies. Image segmentation algorithms separate an image into meaningful homogenous parts depending on a variety of factors including spectral characteristics, shape, texture, and size. Image objects delineated by segmentation are subsequently classified and generalized to define object classifications (Hay et al., 2008).

In essential, the difference between pixel and object representations of an image lies in the used unit, which indicates that most pixel-based techniques in change detection can be transferred to the object-based analysis (Ban et al., 2016b). For example, the algebraic operators including differencing and ratioing used in pixel-based can be performed on object-based change detection as well. The only difference is that instead of using pixels intensity, objects' average intensity should be used as a feature for image analysis tasks. Both supervised and unsupervised mode can be applied as well. In supervised classification, the class identity is built on analyst-selected pixel or segment samples representing training data classes. Unsupervised classification classifiers can adopt

parametric or non-parametric statistical assumptions, hard or soft statistical principles, minimal distance to means or maximum likelihood, and so on. Analysts assign class labels when pixels or segments have been sorted according to cluster types.

It is worth noting that object-based techniques are generally applied on processing very-high spatial resolution (VHR) images, for which the features of objects are normally larger than the pixel of the ground resolution (Strahler et al., 1986). As their name indicated, this type of images has very high spatial resolution, such as up to less than one meter, thus they can capture very detailed spatial structure and texture information of the land surface. Nevertheless, change detection with VHR images severely suffer from the spectral difference of intraclass pixels, thus resulting in considerable ‘pepper and salt’ noises in the change detection map. The object-based approaches can largely overcome this problem and it can also increase computation efficiency due to the processing of objects rather than the pixels. Moreover, image co-registration errors were found to be less sensitive to object-based change detection (Ban et al., 2016a). When changes of the Earth’s surface emerge as distinct objects, the object-based techniques also consider the spatial features rather than merely its spectral, radiometric, and temporal properties (Douglas Stow, 2010). Numerous studies have demonstrated that utilizing spatial contexture information can greatly improve the change detection performance with VHR images (X. Zhang et al., 2017; Zhu et al., 2017).

Corresponding to the classification of pixel-based techniques, the object-based techniques can be classified to three categories as well, i.e., change detection by comparing bitemporal objects, by stacking multi-date data, and by post-classification.

2.2.1. Change detection by comparing bitemporal objects

Change detection by comparing bi-temporal data is similar to pixel-based techniques that compare objects from different dates (Miller et al., 2005). The spectral, spatial, or extracted features of the objects are used for comparison, and displayed the schematic diagram of this category of methods. Object integration with GIS is easy to be implemented with this category of method. Due to the lack of “from-to” change, it makes for searching for spatially related items in multi-temporal images be challenging. Figure 6 displays the schematic diagram of this category of methods.

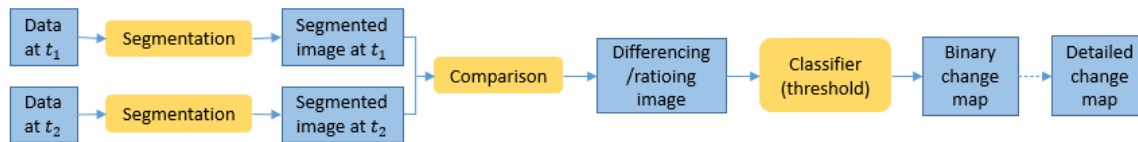


Figure 6. Change detection by comparing bitemporal objects

2.2.2. Change detection by stacking multi-date data

Desclée et al. (Desclée et al., 2006) directly apply image segmentation and classification to stack and composite multi-temporal images. To construct the composite image, co-registered panchromatic, multi-spectral wavebands, or spectrogram were transformed to multi-temporal images. To identify changed objects, a statistical approach is applied. The modified objects are related to the abnormal levels of reflectance difference statistics. A single segmentation produces images of objects that are constantly in scale, geometry, and position between dates. Multitemporal segmentation will cause various abnormalities if there are misregistration and shadowing differences across days (Douglas Stow, 2010). A disadvantage of using single segmentation is that it will not offer new items that may appear at different dates due to any changes. Figure 7 displays the schematic diagram of this category of methods.



Figure 7. Change detection by stacking multi-date data

2.2.3. Change detection by post-classification

Classified object change detection is an extensively used object-based method for generating a change matrix identifying ‘from-to’ changes (Hall et al., 2003). On multi-temporal pictures, the classified object change detection is used to extract and classify objects individually. The grouped items are compared for precise change analysis. This technique was widely used to update object change when given historical maps or GIS data (Hansen et al., 2012; Holland et al., 2008; Xian et al., 2010). The accuracy of the

classification algorithm is directly related with its applications. Figure 8 displays the schematic diagram of this category of methods.

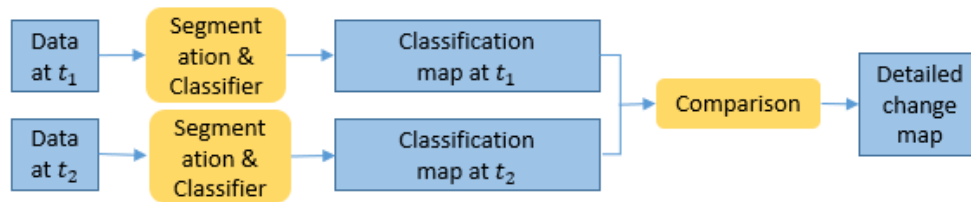


Figure 8. Change detection by post-classification

2.3. Machine learning techniques

Due to the rapid development of computer technology, the machine learning techniques have been increasingly integrated into the research of traditional change detection methods. Essentially, the machine learning can be performed in both pixel and object level. While traditional machine learning, or shallow learning methods are more focused on pixel level, the development of deep learning accelerates object-level vision research.

2.3.1. Change detection with traditional machine learning

Widely used machine learning models include Artificial Neural Network (ANN) ((X. Liu et al., 2002; Pijanowski et al., 2005; Woodcock et al., 2001), Support Vector Machine (SVM) (Huang et al., 2008; Nemmour et al., 2006b). Machine learning aims to generate a precise change information matrix and eliminate the external influence of environmental and atmospheric changes between multi-temporal images datasets. However, choosing a high resolution and adequate training sample imaging dataset for classification, especially for historical imagery dataset classification, might be difficult. When remote sensing training samples of very-high resolutions are not available, it is time-consuming and hard to obtain high-precision classification results, leading to poor change detection outcomes.

ANN algorithms do not make any assumptions about data distribution or independence. It flexibly estimates continuous functions from data without indicating how the outcome are related to inputs mathematically (Im et al., 2005). The trained network is then used to construct a change map using the main dataset. When there is an

irregular distribution of land cover types, ANN technology can offer better results. (Lu et al., 2004). In comparison, SVM, a non-parametric and supervised statistical learning method, is a classification algorithm making no assumptions about the distribution of data and minimizing the structural risk (Vapnik, 2000). Changed and unchanged pixels are treated as binary classification problems when stacked multi-temporal images (Huang et al., 2008). The suitable threshold values generated from the training dataset may distinguish changes and no-change using spectral properties (F. Bovolo et al., 2008). Figure 9 depicts the general workflow of traditional machine learning used for change detection. An example is given in Figure 10 illustrating a binary change detection with SVM and ANN.

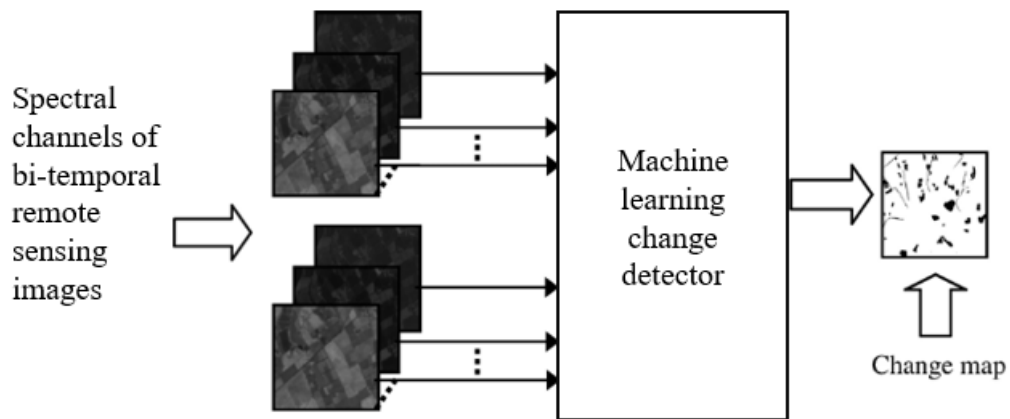


Figure 9. Architecture of machine learning change detector (modified from Nemmour et al. (2006a))

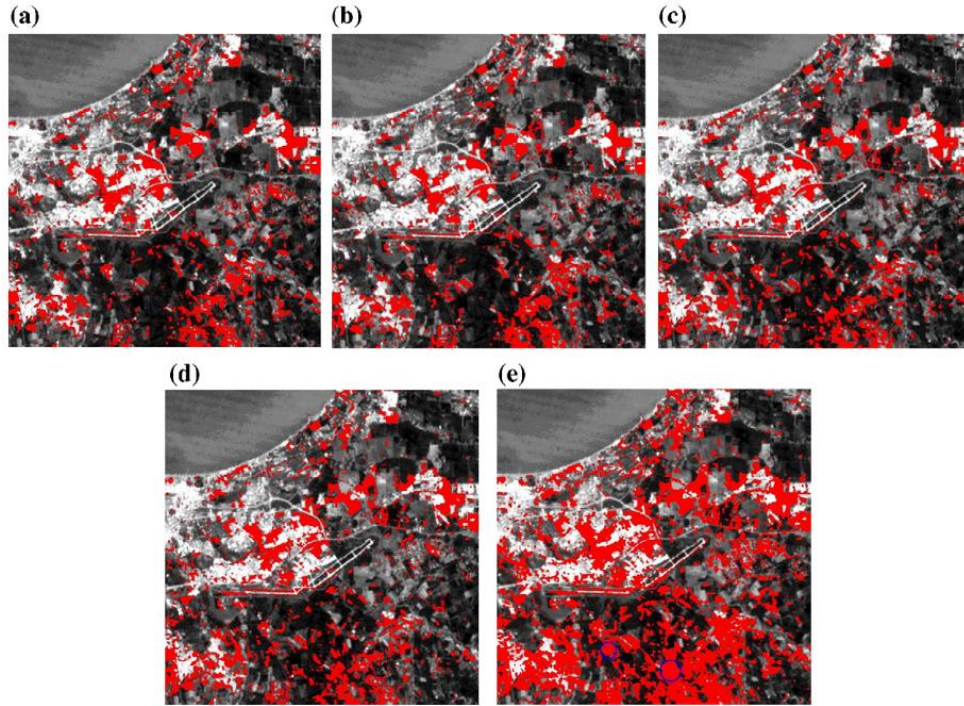


Figure 10. Change maps obtained for the SVM with (a) Polynomial kernel. (b) RBFE kernel, (c) RBFSA kernel and (d) RBFSID kernel and (e) ANN (cited from Nemmour et al. (2006a))

2.3.2. Change detection with deep learning

In recent years, numerous deep learning frameworks for change detection have been developed, such as the convolutional neural network (CNN) (Kemker et al., 2018), recurrent neural network (RNN) (H. Chen et al., 2020), deep belief network (DBN) (Cao et al., 2017), and generative adversarial network (GAN) (Zhao et al., 2020). Instead of segmented the images into objects, such deep learning algorithms divides the image pairs into regular blocks to account for contextual information. It is worth noting that both differencing and stacking strategy can be applied on the deep learning framework as well and examples are given in Figure 11 and Figure 12, respectively.

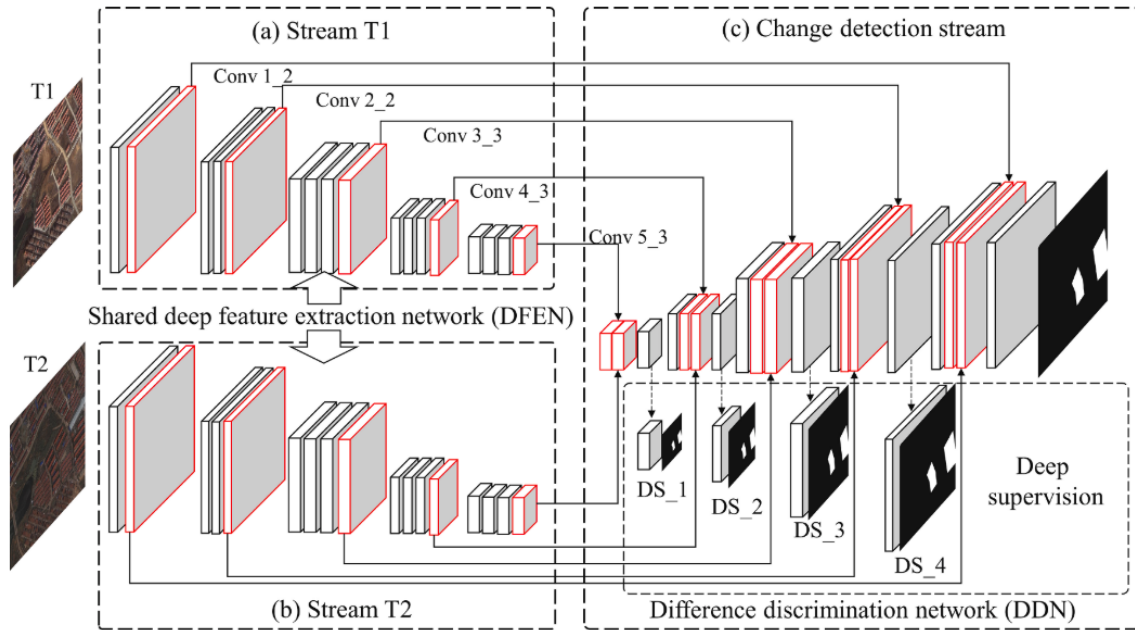


Figure 11. Structure of image stacking for convolutional neural network for change detection (cited from Chenxiao Zhang et al. (2020))

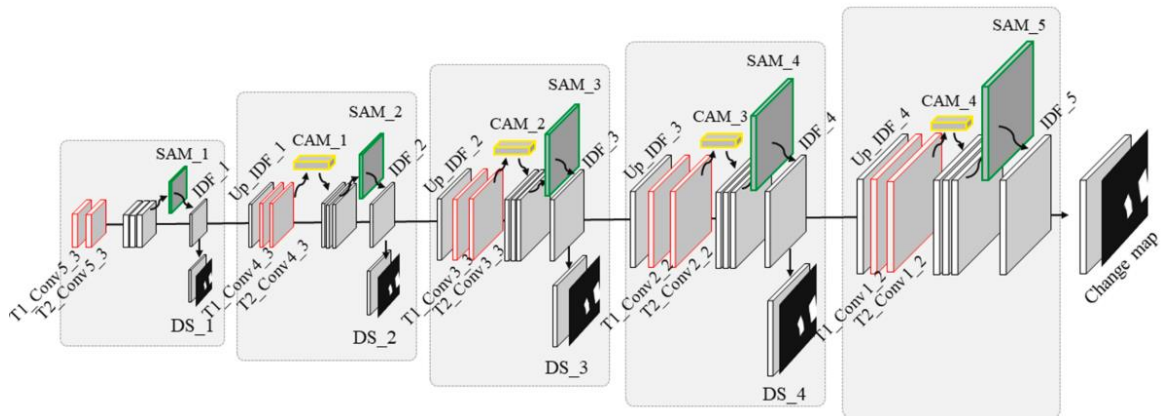


Figure 12. Structure of the difference discrimination network for change detection (cited from Chenxiao Zhang et al. (2020))

In the early stage, small image patches were input into the classification networks to obtain the corresponding categories (P. Chen et al., 2022). Fully convolutional change detection networks applied on entire image have increasingly become the preferred architecture mainly due to the increasing computation ability. The deep learning approach is more robust and has a better generalization ability. As deep learning approaches are normally training with labelling dataset, it thus can learn the “changed” and “unchanged” models directly from the training samples and avoid generating the intermediate images

of change magnitude. Nevertheless, there are two major limitations of this approach. Firstly, the regular shape which is maintained and can partly influence the change detection results. This problem has been addressed by scaling or rotating the direction of training sample and introducing multi-scale convolutional kernel (Zhou et al., 2021). Secondly, a network can achieve relatively high accuracy when provided with sufficient trained samples; however, the labelling of training samples can be time consuming and labour intensive. Transfer models has been implemented as a solution for this problem, which train the initial model on datasets of open source and then refine the model with limited number of real data (J. Liu et al., 2020). Some frequently used open-source datasets constructed for training task of image classification has been given in Shi et al. (2020). An example of change detection with transfer-based deep learning method along with two unsupervised methods of S3VM-based and GAN based is given in Figure 13.

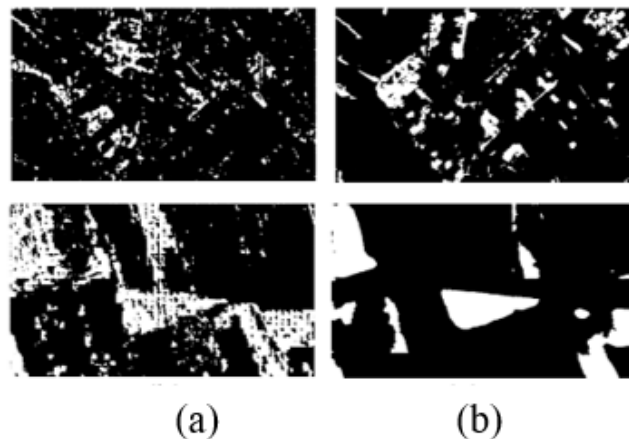


Figure 13. Comparison of change detection with (a) GAN-based, and (b) transfer-based deep learning methods (cited from J. Liu et al. (2020)).

3. A review of DEM change detection using synthetic aperture radar (SAR)

The cloudy and rainy monsoon weather makes land change detection from optical remote sensing extremely challenging in Hong Kong. The Synthetic Aperture Radar (SAR) provides an all-day all-weather operating system, which can penetrate clouds and receive microwave reflectance from the Earth, day and night (Curlander and McDonough, 1991). To overcome the inherent deficiencies of optical systems, SAR images have been used to improve land change detection using images intensities and textures (Gong et al., 2014), the interferometric coherence (Liao et al., 2008), and the combination of SAR and optic sensors (Camps-Valls, et al., 2008). Nowadays with the advancement in both spatial

(up to 1 m) and temporal (within week) resolutions, the involvement of SAR images have significantly contributed to the feasibility and accuracy of retrieving land use land cover (LULC) products from satellite remote sensing techniques. In particular, the coherence map derived from interferometric SAR (InSAR) (Bamler and Hartl, 1998) reveals minor and sensitive ground change information, from which the spatiotemporal coherence behavior can be analyzed to identify and retrieve different ground features (Jiang et al., 2017). However, both the intensity (amplitude) and coherence can only reflect shape-related ground changes. Taking advantages of the precise repeat track design of SAR satellites, InSAR become one of the few remote sensing tools that can reflect geometry information, e.g., detecting spatially detailed ground topography (elevation) and deformation (Bürgmann et al., 2000). Regardless the noise effects, the interferometric phase of two SAR images contains the phase components contributed from the ground topography and ground deformation (Bamler and Hartl, 1998). The topography phase can be converted to the ground elevation, i.e., generating a Digital Elevation Model (DEM), based on the geometry between SAR satellite and the earth (Crosetto, 2002).

Launched in February 2000, the Shuttle Radar Topography Mission (SRTM) by NASA generated the first near-global scale DEM (56° S to 60° N) product via single-pass interferometry (Farr et al., 2007). In 2009, another representative InSAR-based global DEM was released jointly by NASA and Japan's Ministry of Economy, Trade and Industry (METI), i.e., ASTER GDEM V1 (Reuter et al., 2009), with its subsequent version ups of ASTER GDEM V2 and ASTER GDEM V3 released in 2011 and 2019, respectively. Compared to the conventional 2D change detection, these InSAR derived 3D data provides volumetric dynamics to facilitate more change detection applications with better accuracy. Therefore, it is possible that ground changes can be featured by InSAR derived DEMs, via tracking the topography changes. Earlier studies have used InSAR DEMs to estimate large scale glacier elevation changes (Muskett et al., 2003), 3D glacier motion map (Gudmundsson et al., 2002), landslides identification (Huang et al., 2015), volumetric change during volcano eruption (Kubanek et al., 2015), etc. In recent years, the German Aerospace Center (DLR) launched the X-band TanDEM-X mission and has acquired data for the generation of two versions of high-resolution global digital elevation models, i.e., TanDEM-X DEM (Rizzoli, et al., 2017) and TanDEM-X Change

DEM (Lachaise et al., 2020). The TanDEM-X Change DEM product has covered majority of the land areas (Figure 14), which enables the retrieval of even small terrain changes on global scales with unprecedented resolution (Bachmann et al., 2018). Fine scale applications have been made related to, e.g., industrial activities (Lachaise et al., 2020), mining production (Figure 15), forestation/deforestation (Schweisshelm and Lachaise, 2021), etc. In combining with the old SRTM DEM, the TanDEM-X products and can also support inter-decadal terrain change analysis, for example biomass estimation (Solberg et al., 2018). In Hong Kong, considering the intensive vegetation coverage on most of its natural terrains, the long wavelength L-band SAR data is more suitable for DEM change detection from InSAR. In particular, the newly launched L-band LUTAN-1 satellite by China will provide continuous data for future studies in the Guangdong-Hong Kong-Macao Greater Bay Area.

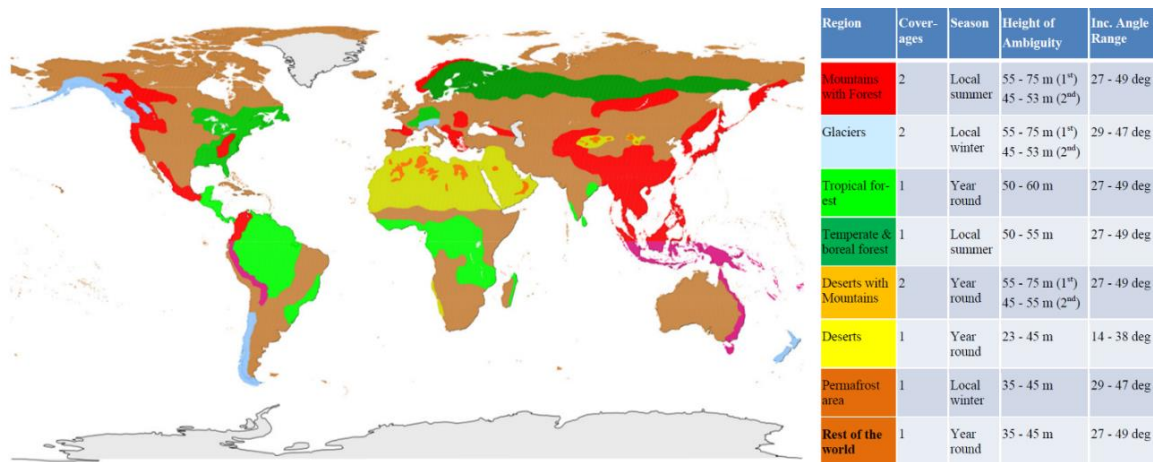


Figure 14. Detected acquisition areas for the TanDEM-X Change DEM acquisition phase (from 2017-09-21 until mid-2020), with acquisitions parameters in the table (cited from Bachmann et al., 2018).

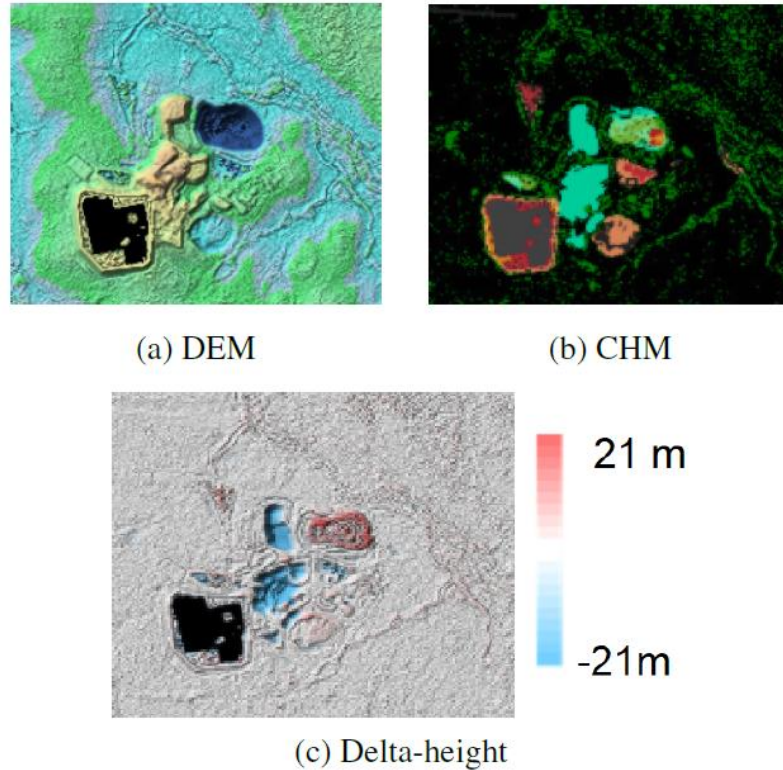


Figure 15. DEM difference reveals terrain changes in a mine structure (cited from Schweishelm and Lachaise, 2021).

4. A review of land cover land use product in Hong Kong

The LUM has undergone four major generations. The differences in the four generations mainly consist in three aspects including the data sources used, methodologies used for classification and change detection, and the land use classification system.

From 1993 to 2001, the land utilization map (LUM) and Land Utilization Table (LUT) is basically produced manually by making use of secondary data gathered from various government departments and by conducting field survey for places where no secondary data are available (CUHK, 2001).

Starting from 2001, the land utilization plan designed by the CUHK in 2001 (hereafter CUHK 2001) was used for generation of LUM and LUT (Planning Department Hong Kong, 2001). They incorporate the satellite images and take advantage of digital image analysis for automatic image classification. An integration of both remote sensing images and other sources of information (e.g., GIS data) is used considering that the remote

sensing images has limitations on land use classification in urban area that are defined according to human activities. They divide the entire territory of Hong Kong into three different regions with adoption of different methods. Specifically, it uses the existing land use plans with digital image analysis for “unused land” on the areas of Hong Kong, Kowloon and Tsuen Wan Metro (CUHK, 2001). It updates the existing land use plans based on change detection method of principal component analysis with satellite data (i.e., Landsat-7 in 2000 and SPOT-2 HRV2 image in 1997) for the New Towns area. As for the rural New Territories, it adopted maximum likelihood classification (MLC) for digital image classification about specific land cover classes with Landsat-7 ETM image (CUHK, 2001).

The CUHK, 2001 was improved by CUHK, 2007. The MLC classification technique used in CUHK 2001 is subject to normal distribution for the training data set and it did not consider texture features. They improve the MLC based on logistic regression where the dependent variables are not required to be normally distributed, and it integrate the traditional spectral, texture and topographical parameters for LULC classification. The spectral parameters include bands 1-4 and the derive NDVI from SPOT 5 imagery. The texture parameters derive from multispectral images was revealed to be a very valuable source of spatial information and an important clue for land cover classification. It includes contrast, correlation, uniformity, and homogeneity. Topological indicator was represented by digital elevation model (CUHK, 2007).

In 2003, sustainable operation of future landuse updating applications within the LUM and LUT for the Pearl River Delta (PRD) Region was carried out by the Planning Department aiming to update the Territorial Development Strategy (TDS) entitled “Hong Kong 2030: Planning Vision and Strategy” (BUHK, 2003). It integrates various sources of information, including both remote sensing images and GIS data, with the primary data source of Landsat ETM images. To maximize the usage of available data and to minimize the demand on resource and time, it integrates image auto-classification, visual interpretation and GIS processing together with the image classification being the core of data processing (BUHK, 2003).

However, the abovementioned methodologies for producing LUM HK and LUM PRD by the Planning Department are mainly pixel-based, which have two limitations, Firstly,

it cannot resolve the high spectral variation within the same land cover, and the spectral confusion among different land covers. Secondly, classification using only pixel-based spectral features result in a large number of “salt and pepper” outputs and the inherent spatial information is underestimated. Considering the defects in the previous LUM products, PolyU group commissioned by the Hong Kong Planning Department in 2013 (hereafter PolyU 2013) to produce LUM for Hong Kong and PRD incorporates an additional Multi-scale Object Oriented Segmentation with decision tree Classification (MOOSC) (Nichol and Wong, 2008) method, which is a complementary classification method based on parcels instead of pixels (PolyU, 2013). It creates regional patches that represent one class within a patch and can give a better description and classification of rural vegetation since it groups the pixel in segments and minimizes the internal variance within classes. Thus, the variability of pixels within a class can be reduced. It can significantly reduce the “salt and pepper” pixel problem from pixel-based classifiers. In order to increase the band dimensionality, more band channels including the original multispectral bands, Normalized Difference Vegetation Index, Soil-Adjusted Vegetation Index (SAVI), Modified Soil-adjusted Vegetation Index (MSAVI), Chlorophyll index, a DEM raster band and three texture bands were input to the classifiers (PolyU, 2013). The SPOT-5, SPOT-6 and WorldView2 images are employed for the land cover classification, among which the WorldView2 images were particularly used for discrete heterogeneous land covers. The Landsat-8 satellite images were used for the entire PRD region.

As a critical part in LUM generation, the categorization of land use or land use classification systems in the four generations of LUM have minor discrepancies, which is revised continuously mainly due to the updated users’ demanding, sources of land use information gathered, spatial and spectral resolution of remote sensing images, scales of land use plan, as well as the compatibility with land use information derived at different scales and required by different agencies (CUHK, 2001, 2003; BUHK, 2003; PolyU, 2013).

It is recommended that a comprehensive review on the Land Utilization Plan and Land Usage Table should be undertaken every five years considering the accumulated error propagation, updated users demanding, and the availability of new satellite images of improved resolution as well as advancements in image processing and GIS technique.

5. Remote sensing imageries used for change detection

The change detection was facilitated by the employment of medium-resolution, high-resolution or very-high-resolution images. One study used MODIS product data (i.e., MCD12Q1v006 dataset) that provides global land use and land cover maps every year at 500m spatial resolution to detect LULC change over the Greater Bay Area (GBA) including Hong Kong between 2001 and 2019 (Wang et al., 2021), which covers a large area and long time period with a relatively coarse spatial resolution. To achieve a better detection resolution, Landsat Thematic Mapper (TM) images were widely used (Wang & Li, 2011; Wong et al., 2017). Also, atmospherically corrected Landsat images with 30 m spatial resolution, including Landsat 5 TM, 7 ETM+, and 8 OLI level 2, were collected for the study in Hong Kong (Hasan et al., 2019; Hasan et al., 2020). As a special dataset, nighttime light time series (NLT) data were acquired for detecting GBA LULC changes, which has a relatively coarse spatial resolution at 1 km obtained from the Defense Meteorological Satellite Program (DMSP) with the Operational Linescan System (OLS) version 4 (Hasan et al., 2019; Hasan et al., 2020). As a combination of optical images from Landsat ETM+ (30m) and Synthetic-aperture radar (SAR) images from ENVISAT ASAR (75m), they were used for Guangzhou, SPOT-5 (10m) and ENVISAT ASAR (10m) were used for Shenzhen, and SPOT-5 (10m) and TerraSAR-X (3m) were used for Hong Kong to extract impervious surfaces effectively (Zhang et al., 2014). Furthermore, as Hong Kong has one of the highest density of urban areas across the globe, detecting minor LULC changes becomes essential to utilizing precious land and space effectively, which requires remote sensing images having very high-resolution that can be acquired from advanced satellites, such as WorldView-3 with spatial resolution finer than 1m (DigitalGlobe, 2021).

Overall, satellite data normally have different spatial and spectral resolutions. The selection of the satellite images should consider not only the image spatial resolution, but also the spectral bands that should encompass at least blue, green, red and near-infrared bands. Basically, the satellite images can be grouped into two categories. The first group is very high spatial (VHS) resolution data, such as the images captured by IKONOS, QuickBird, WorldView, FLOCK, SPOT and GF satellites. Such VHS images are only

available for commercial use in Hong Kong and they resemble aerial photos and are particularly good for visual interpretation. The second group is high spatial resolution images with spatial resolution ranging from 10 to 30m. The satellites of Landsat, Sentinel, and HJ-2 are representatives. The third group is medium spatial resolution satellites, e.g., Terra and Aqua with MODIS sensors, SNPP and NOAA-20 with VIIRS sensors, and Sentinel-3 with OLCI sensors. Table 1 illustrates major characteristics of satellite data relevant to the LUM production.

Table 1. Major characteristics of satellite data

Type	Satellite (Sensor)	Waves (nm)	Spatial res. (m)	Temporal res.	Passing time	Lifetime	Application
Very high spatial resolution	IKONOS (OSA)	PAN 490 565 680 810	0.82 3.30	Global coverage in 6 months in daylight	SSO 10:30 desc	1999 - 2015	Biomass, fraction of absorbed PAR, fraction of vegetated land, land cover, leaf area index, normalized difference vegetation index, vegetation type
	QuickBird (BGIS-2000)	PAN 485 560 660 830	0.60 2.40	Global coverage in 6 months in daylight	SSO 10.30 desc	2001 - 2015	Biomass, fraction of absorbed PAR, fraction of vegetated land, land cover, leaf area index, normalized difference vegetation index, vegetation type
	WorldView-1 (WV60)	PAN	0.50	Global coverage in 6 months in daylight	SSO 13:30 desc	2007 - 2022	Fire fractional cover
	WorldView-2 WorldView-3 (WV110)	PAN 425 480 545 605 660	0.46 1.84	Global coverage in 6 months in daylight	SSO 10.30 desc	2009 - 2022 2014 - 2022	Biomass, fraction of absorbed PAR, fraction of vegetated land, land cover, leaf area index, normalized difference vegetation index, vegetation type

		725 832 950					
	WorldView-4 (SpaceView-110)	PAN 480 545 672 850	0.31 1.24	Global coverage in 6 months in daylight	SSO 10:30 desc	2016 - 2019	Biomass, fraction of absorbed PAR, fraction of vegetated land, land cover, leaf area index, normalized difference vegetation index, vegetation type
	FLOCK	485 545 630 820	3.7	The full constellation of satellites provides daily coverage. 3.5 months for a single satellite.	SSO 10:30 desc	2014 - 2040	Fire fractional cover, Fraction of vegetated land, land cover, normalized difference vegetation index, soil type, vegetation type
	SPOT-6 SPOT-7 (NAOMI)	PAN 485 565 655 825	2 8	Global coverage in 1 months. Minimum revisit time for a specific area: 3 days	SSO 10:30 desc	2012 - 2022 2014 - 2024	Biomass, fraction of absorbed PAR, fraction of vegetated land, land cover, leaf area index, normalized difference vegetation index, vegetation type
	GF-1 GF-6	PAN 485	2 8	Global in 1 month	SSO 10:30 desc	2013 – 2022 2018 - 2026	Biomass, fraction of absorbed PAR, fraction of

	(PMS)	555 660 830					vegetated land, land cover, leaf area index, normalized difference vegetation index, vegetation type
	GF-2 GF-7 GF-8 GF-9 GF-10 GF-11 GF-14 (PMS-2)	PAN 485 555 660 830	0.75 3	Global in 2 months for single satellite. For full Jilin-1 constellation of 138 satellites this achieves images every 10 mins.	SSO 10:30 desc	2014 - 2022 2019 - 2027 2015 - 2023 2015 - 2023 2019 - 2027 2018 - 2027 2020 - 2028	Biomass, fraction of absorbed PAR, fraction of vegetated land, land cover, leaf area index, normalized difference vegetation index, vegetation type
High spatial resolution	Landsat-7 (ETM+)	PAN 480 560 660 830 1650 2200 nm 11.45 μm	15 30 60	Global coverage in 16 days, in daylight.	SSO 10:00 desc	1999 - 2022	Biomass, fraction of absorbed PAR, fraction of vegetated land, land cover, leaf area index, normalized difference vegetation index, vegetation type
	Sentinel-2A Sentinel-2B Sentinel-2C Sentinel-2D	443, 490, 560, 665, 705, 783, 842, 865,	60, 10, 10, 10, 20, 20, 20, 10, 20, 60, 60, 20,	Global coverage in 10 days, in daylight	SSO 10:30 desc	2015 - 2022 2017 - 2024 2024 - 2031 2025 - 2032	Biomass, fraction of absorbed PAR, fraction of vegetated land, land cover, leaf area index, normalized

	(MSI)	945, 1375, 1610, 2190	20				difference vegetation index, vegetation type
	HJ-2A HJ-2B (WVC-2)	470 560 660 830	16	Global coverage in 4 days	SSO 10:30 desc	2020 - 2025 2020 - 2025	Biomass, fraction of absorbed PAR, fraction of vegetated land, land cover, leaf area index, normalized difference vegetation index, vegetation type
Medium spatial resolution	Terra Aqua (MODIS)	645, 858, 469, 555, 1240, 1640, 2130, 412, 443, 488, 531, 551, 667, 678, 748, 870, 905, 936, 940, 1375 and the other 16	250 (band 1-2) 500 (band 3-7) 1000 for the other bands	Global coverage nearly twice/day (long-wave channels) or once/day (short-wave channels)	SSO 10:30 desc 13:30 asc	1999 - 2023 2022 - 2025	Ocean colour, vegetation, aerosol, cloud properties, Earth surface albedo, oil spill cover, land cover

		infrared bands					
SNPP NOAA-20 (VIIRS)	412, 445, 488, 555, 672, 746, 865, 1240, 1378, 1610, 2250 nm, 3.70, 8.55, 10.763, 12.013 µm 700, 640, 865, 1610 nm, 3.74, 11.45 µm	750 (band 1-16) 375 (band 17-22)	Global coverage twice/day (IR and day/night VIS/NIR channel) or once/day (VIS)	SSO 13:25 asc	2011 - 2014 2017 - 2027	Ocean colour, vegetation, aerosol, cloud properties, Earth surface albedo, oil spill cover, land cover	
Sentinel-3A Sentinel-3B Sentinel-3C Sentinel-3D (OLCI)	400, 412.5, 442.5, 490, 510, 560,	300	Global coverage in 2 days, in daylight	SSO 10:00 desc	2016 - 2035 2018 - 2025 2024 - 2031 2028 - 2035	Ocean colour, vegetation, aerosol, cloud properties, Earth surface albedo, oil spill cover, photosynthetically active	

		620, 665, 673.75, 681.25, 708.25, 753.75, 761.25, 764.375, 767.5, 778.75, 865, 885, 900, 940, 1020					radiation
	GF-4 (GF-4 imager)	PAN MWIR	50 400	Local coverage over China at minute-level	GEO	2015 - 2023	Fire fractional cover Fire radiative power Fire temperature Land surface temperature Sea surface temperature
SAR	Sentinel-1A Sentinel-1B Sentinel-1C Sentinel-1D (SAR)	C-band SAR	Stripmap 4*5 m2 ScanSAR - Interferometric 5*20 m2	Global coverage in 5 days for the 'Extra-wide swath' mode (duty cycle 70 %); in longer periods for other operation modes (duty	SSO 06:00 desc	2014 – 2022 2017 – 2024 2024 – 2031 2025 – 2032	Glacier cover, Glacier motion, Glacier topology, ice sheet topography, land surface topography, sea-ice cover, sea-ice type

			ScanSAR - Extra-wide swath 25*80 m2 Wave (WV) 20*5 m2	cycle 30 %), up to 3 months			
GF-3 GF-12 (SAR-C)	C-band SAR with 12 operating mode	1	Global in one week in the large-swath mode	SSO 06:00 desc	2016 – 2024 2019 - 2027	Glacier cover, Glacier motion, Glacier topology, ice sheet topography, land surface topography, sea-ice cover, sea-ice type	
TerraSAR-X TanDEM-X (SAR-X)	X-band	1 to 16 m depending on operation mode	Minimum revisit time of 2.5 days for a selected location	SSO 06:00 desc	2007 – 2024 2010 - 2026	Fraction of vegetated land, glacier motion, glacier topology, land cover, land surface topology, soil moisture at surface, soil type, vegetation type	
ENVISAT (ASAR)	C-band	30 to 1000 m depending on operation mode	Global coverage in 5 day for the ‘global monitoring’ mode	SSO 06:00 desc	2002-2012	glacier motion, glacier topology, land cover, land surface topology, soil moisture at surface, sea-ice cover, sea-ice type	

6. Thematic accuracy assessment

Accuracy assessment is required to provide users on the confidence level that this map can be used as errors may occur during the LUM compilation process, which includes i) cartographic generalization of the LUM, ii) misclassification in remote sensing classification and iii) change detection from the previous map. Accuracy assessment is thus a necessary step in LUM generalization. It is performed by selecting sample pixels and checking with the reference information to determine overall accuracy of the LUM map as well as individual land use categories. The reference information is normally the sample points that can be collected from existing LUM or identified manually through ground survey, interpretation of aerial photos, very high-resolution images. Such sample points should be randomly selected before data processing tasks performed to avoid bias from human operator. The comprehensiveness of classes should be checked to ensure that the selected sample points will adequately cover all classes. It should be noted that part of the samples is used in the training processing of image classification procedure, while the remaining samples are used as the test samples for accuracy assessment.

Various measures that used in the classification domain can normally be used in the change detection, which normally includes confusion matrix or error matrix, overall accuracies, kappa coefficient, as well as the producer's and user's accuracy of each class.

A confusion matrix is generated by comparing a number of sample sites on the map to their equivalent locations in an appropriate source of higher accuracy. The columns in the matrix define the classes in the reference data, and the rows define the classes in the data being evaluated for accuracy. The diagonal elements of the matrix indicate correct classifications. The values in the cells in the table indicate how well the classified data agree with the reference data. With the samples pixels, it is possible to derive the overall accuracy, user's accuracy (or commission error) and producer's accuracy (omission error) of individual category from the error matrix.

The overall accuracy is computed as a ratio of the number of correctly classified samples to the total number of samples, which is commonly used to assess the accuracy level of the entire classification. User's accuracy of a particular land use category is computed as the ratio of the number of correctly classified samples in that category to the

total number of samples belong to the same category from the classified map (the row total). It is a measure of the commission error for each category and represent the probability of a pixel classified on the map being the actual category on the ground. Producer's accuracy of a particular land use category is computed as the ratio of the number of correctly classified samples in that category and the total number of samples being to the same category (the column total) from the reference information. This measure indicates the probability of a reference pixel being corrected classified.

However, the overall accuracy can be misleading as an index as a certain number of correct classifications will occur by change, even in the most uncertain situations. The Kappa index with values ranging between 0 and 1 is expected under maximum uncertainty, which is computed as:

$$\hat{k} = \frac{P_{correct} - P_{chance}}{1 - P_{chance}}$$

where $P_{correct}$ is the proportion of correctly classified entries and P_{chance} is the proportion of samples expected to be correctly classified by change formulated as:

$$P_{chance} = \sum_{i=1}^n P_{row(i)}P_{column(i)}$$

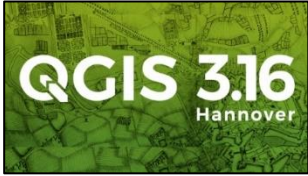
where $P_{row(i)}$ is the proportion of total entries that are in row i, $P_{column(i)}$ is the proportion of all entries that are in column i, and n is the total number of rows or columns.




7. Common software and programming language for change detection


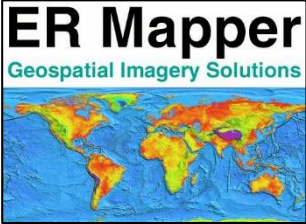


7.1. Common Software for change detection






Various softwares are available for the data processing and analysis for LULC change detection. Table 2 lists the commonly used software that can be used for LULC change detection.

Table 2. Common software for LULC change detection.

Software name	Description	Symbol
QGIS	QGIS consists of a variety of user-friendly opensource functions and plugins for LULC change detection, including RS image visualizing, editing,	

	<p>and analyzing, and composing printable maps.</p>	
<p>ENVI</p>	<p>ENVI is a commonly used software for image processing and analyzing. Plenty of data types can be supported by it, such as multi- and hyper-spectral images, 3D LiDAR point cloud as well as SAR and FMV datasets. Expert-level results can be achieved by simple operations. In addition, it can work with much other software like ArcGIS.</p>	
<p>ERDAS IMAGINE</p>	<p>ERDAS IMAGINE is another world's leading software for RS. Simple scenes combined with powerful algorithms and data processing functions enable users to focus on analyses. Besides, multiple classification methods were incorporated into this software, including pixel-based and object-based classification, machine learning, and deep learning classification methods.</p>	
<p>Trimble eCognition</p>	<p>eCognition is designed to robustly, accurately, and rapidly extract information from any kind of geospatial data by emulating the cognitive power of the human mind. The meaning from objects' connotations and mutual relationships throughout various input data is distilled for depth analysis and interpretation.</p>	



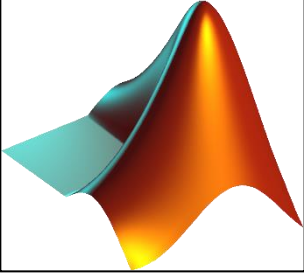

<p>ESRI ArcGIS</p>	<p>ArcGIS is an integrated geospatial software based on a GIS system for viewing, editing, managing, and analyzing geographic data. A family of client software is contained, including ArcMap, ArcCatalog, ArcToolbox, ArcScene, and ArcGlobe. ArcCatalog is for dataset browsing, previewing and metadata management. ArcMap is for editing and querying geospatial data and creating maps. ArcToolbox contains a large number of geoprocessing, data conversion and analysis tools. ArcScene and ArcGlobe allow users to view GIS data in 3D and conduct 3D analyst.</p>	
<p>Er Mapper</p>	<p>Er Mapper is a professional software for RS and GIS data processing and exploitation. It can provide real-time responses, immediately processing and enhancing options for users.</p>	
<p>3D GIS</p>	<p>3D GIS is designed to improve the effectiveness of data and information in cities based on geographic techniques.</p>	
<p>IDRISI</p>	<p>IDRISI offers many GIS analysis tools to raster data and special graphical modeling environments. In addition, extremely flexible APIs allow users to achieve better processing and analysis.</p>	

PCI Geomatics	PCI Geomatics delivers a lot of solutions for more informed and faster decisions based on RS and GIS data and analysis.	
GRASS GIS	GRASS GIS is a opensource software for powerful raster, vector, and geospatial processing engines. A temporal framework and a Python API are provided for rapid programming.	
SAGA GIS	SAGA GIS is designed for easy and effective implementation of spatial algorithms. It delivers a fast-growing set of geoscientific methods.	
gvSIG	gvSIG is a professional software for spatial data infrastructures, mobile solutions, and sectoral solutions. It includes a field app, 3D capabilities, and a desktop application.	
ILWIS	ILWIS is a opensource GIS and RS software for digitizing, editing, and displaying of geographic data, as well as classification, enhancements, and spectral band manipulation of images.	

7.2. Programming Language for change detection

Programming can help to process the data more effectively and efficiently, including RS images and geospatial datasets. Table 3 lists the commonly used programming language that can be used for LULC change detection.

Table 3. Programming language for LULC change detection

Programming language	Description	Symbol
Python	Python is a worldwide and flexible programming language for RS and GIS. A set of libraries and algorithms for image processing and geospatial data analysis are incorporated.	
R	R is another worldwide and flexible programming language. Different from python, R provides more easy-used statistical methodologies.	
Matlab	Matlab is good at metric processing, so it provides many algorithms for rapid image processing. It is one of the preferred languages for applied mathematics and engineering.	
IDL	IDL is incorporated with ENVI software. It provides robust support for mathematical and statistical programming.	

8. Discussion and conclusion

During the process of producing the land utilization map, the processing speed can be greatly improved when only the changes are represented rather than all the information of both images are exposed to the interpreter or human viewer (Singh, 1989). Therefore, change detection is of great importance which has been used in diverse applications, such as land use change analysis, monitoring of shifting cultivation, assessment of deforestation, change study in vegetation phenology, seasonal changes in pasture production, damage assessment, crop stress detection, disaster monitoring, snow-melt

measurements, day/night analysis of thermal characteristics and other environmental changes (Singh, 1989).

The overall workflow of change detection consist of data acquisition, data preprocessing, a change detection algorithm, and an accuracy evaluation (Asokan et al., 2019). LULC change detection requires accurate geometric co-matching and atmospheric correction between images captured at different times. To achieve high-quality change detection, it is important to select proper images captured by various sensors, define suitable change classes, and employ adaptive methods. Methods employed should be dedicated to reduce the effect from the external factors of atmospheric conditions, moisture conditions, illumination and sensor calibration. Additionally, precise geometric registration of images is required which can be achieved by taking more accurate ground control points, or methods can be explored to bypass the requirement of the registration problem. Thus, appropriate selection of change detection techniques is crucial to obtain an accurate classification of the LULC changes.

Some image processing methods, such as image differencing, image ratioing, which only deliver binary information, i.e., change versus no-change. If a study requires a detailed change matrix, more complicated techniques, such as post-classification, multitemporal-object change detection, and CNN, should be considered. An alternative method to determine a change detection can be relied on image analysis. Many standard pixel-based approaches are insufficient for processing high-resolution remote sensing images, while object-based method can be determined more effectively. There are a large number of algorithms essentially utilizing the pixel- and object-based approaches, which have been developed to be adapted into different scenarios. Each method has its own merits and demerits. The change detection methods normally are used jointly to handle the problem of real-word land utilization mapping as no single technique is sufficient for evaluating land use change information of all land types. The performance of various methods under different environments must be evaluated quantitatively to provide sufficient support for remote sensing specialists and resources managers to apply in an operational monitoring program.

There is an increasing demand for developing new algorithms to provide reliable LULC change detection since new RS data are continuously generated from newly

developed sensors. Despite the development of several change detection strategies, it remains challenging to choose a suitable method to achieve detection of study areas accurately, such as urban transformation, deforestation, desertification, and wetland change, etc. This study provides a relatively holistic review for land use land cover change detection algorithms, which is beneficial for the selection of appropriate change detection methods in future land utilization map generation. Thus, the authors suggest that comprehensive evaluation and analysis on all previously discussed components can help select an appropriate change detection method. Meanwhile, different change detection methods can be used for the same study area so that cross comparison can be implemented to determine result based on visual and/or quantitative accuracy assessment more reliable and accurate. New technologies are under research and developments, it is essential to keep track of these developments and adopt suitable ones for cost effectiveness and efficiency.

Reference

- Achard, F., Eva, H. D., Stibig, H.-J., Mayaux, P., Gallego, J., Richards, T., & Malingreau, J.-P. (2002). Determination of Deforestation Rates of the World's Humid Tropical Forests. *Science*, 297(5583), 999-1002.
- Akbari, V., Doulgeris, A. P., & Eltoft, T. (2014). Monitoring Glacier Changes Using Multitemporal Multipolarization SAR Images. *IEEE transactions on geoscience and remote sensing*, 52(6), 3729-3741.
- Alphan, H. (2011a). Comparing the utility of image algebra operations for characterizing landscape changes: The case of the Mediterranean coast. *J Environ Manage*, 92(11), 2961-2971.
- Alphan, H. (2011b). Comparing the utility of image algebra operations for characterizing landscape changes: The case of the Mediterranean coast. *Journal of Environmental Management*, 92(11), 2961-2971.
- Alphan, H., Doygun, H., Unlukaplan, Y. I. J. E. m., & assessment. (2009). Post-classification comparison of land cover using multitemporal Landsat and ASTER imagery: the case of Kahramanmaraş, Turkey. *151(1)*, 327-336.

- Alqurashi, A., & Kumar, L. (2013). Investigating the use of remote sensing and GIS techniques to detect land use and land cover change: A review. *Advances in Remote Sensing*.
- Asokan, A., & Anitha, J. (2019). Change detection techniques for remote sensing applications: a survey. *Earth Science Informatics*, 12(2), 143-160.
- Ban, Y., & Yousif, O. (2016a). Change Detection Techniques: A Review. In (pp. 19-43). Cham: Cham: Springer International Publishing.
- Ban, Y., & Yousif, O. (2016b). Change Detection Techniques: A Review. In Y. Ban (Ed.), *Multitemporal Remote Sensing: Methods and Applications* (pp. 19-43). Cham: Springer International Publishing.
- Ban, Y., Yousif, O. A. J. I. J. o. S. T. i. A. E. O., & Sensing, R. (2012). Multitemporal spaceborne SAR data for urban change detection in China. 5(4), 1087-1094.
- Benz, U. C., Hofmann, P., Willhauck, G., Lingenfelder, I., & Heynen, M. (2004). Multi-resolution, object-oriented fuzzy analysis of remote sensing data for GIS-ready information. *ISPRS journal of photogrammetry and remote sensing*, 58(3), 239-258.
- Bontemps, S., Bogaert, P., Titeux, N., & Defourny, P. (2008). An object-based change detection method accounting for temporal dependences in time series with medium to coarse spatial resolution. *Remote sensing of environment*, 112(6), 3181-3191.
- Bovolo, F., Bruzzone, L., & Marconcini, M. (2008). A Novel Approach to Unsupervised Change Detection Based on a Semisupervised SVM and a Similarity Measure. *IEEE transactions on geoscience and remote sensing*, 46(7), 2070-2082.
- Bovolo, F., Bruzzone, L. J. I. T. o. G., & Sensing, R. (2006). A theoretical framework for unsupervised change detection based on change vector analysis in the polar domain. 45(1), 218-236.
- Brondizio, E. S., Moran, E. F., Mausel, P., & Wu, Y. (1994). Land use change in the Amazon estuary: Patterns of Caboclo settlement and landscape management. *Human Ecology*, 22(3), 249-278.
- Campbell, J. B., & Wynne, R. H. (2011). *Introduction to remote sensing*: Guilford Press.
- Cao, G., Wang, B., Xavier, H.-C., Yang, D., & Southworth, J. (2017). A new difference image creation method based on deep neural networks for change detection in remote-sensing images. *International Journal of Remote Sensing*, 38(23), 7161-7175.

- Chen, H., Wu, C., Du, B., Zhang, L., & Wang, L. (2020). Change Detection in Multisource VHR Images via Deep Siamese Convolutional Multiple-Layers Recurrent Neural Network. *IEEE Transactions on Geoscience and Remote Sensing*, 58(4), 2848-2864.
- Chen, P., Zhang, B., Hong, D., Chen, Z., Yang, X., & Li, B. (2022). FCCDN: Feature constraint network for VHR image change detection. *ISPRS Journal of Photogrammetry and Remote Sensing*, 187, 101-119.
- Chen, X., Vierling, L., & Deering, D. (2005). A simple and effective radiometric correction method to improve landscape change detection across sensors and across time. *Remote Sensing of Environment*, 98(1), 63-79.
- Dawelbait, M., & Morari, F. (2012). Monitoring desertification in a Savannah region in Sudan using Landsat images and spectral mixture analysis. *Journal of arid environments*, 80, 45-55.
- Desclée, B., Bogaert, P., & Defourny, P. (2006). Forest change detection by statistical object-based method. *Remote Sensing of Environment*, 102(1), 1-11.
- Dewan, A. M., & Yamaguchi, Y. (2009). Land use and land cover change in Greater Dhaka, Bangladesh: Using remote sensing to promote sustainable urbanization. *Applied Geography*, 29(3), 390-401.
- Estes, J. E., Stow, D., & Jensen, J. R. (1982). Monitoring land use and land cover changes. *Remote sensing for resource management*, 100-110.
- Gamba, P., Dell'Acqua, F., & Lisini, G. (2006). Change Detection of Multitemporal SAR Data in Urban Areas Combining Feature-Based and Pixel-Based Techniques. *IEEE transactions on geoscience and remote sensing*, 44(10), 2820-2827.
- Gordon, S. I. (1980). Utilizing LANDSAT imagery to monitor land-use change: A case study in ohio. *Remote Sensing of Environment*, 9(3), 189-196.
- Hall, O., & Hay, G. (2003). A multiscale object-specific approach to digital change detection. *International Journal of Applied Earth Observation Geoinformation*, 4(4), 311-327.
- Hansen, M. C., & Loveland, T. R. (2012). A review of large area monitoring of land cover change using Landsat data. *Remote Sensing of Environment*, 122, 66-74.

- Hay, G. J., & Castilla, G. (2008). Geographic Object-Based Image Analysis (GEOBIA): A new name for a new discipline. In (pp. 75-89). Berlin, Heidelberg: Berlin, Heidelberg: Springer Berlin Heidelberg.
- Holland, D., Sanchez-Hernandez, C., & Gladstone, C. (2008). *Detecting changes to topographic features using high resolution imagery*. Paper presented at the Proceedings of the ISPRS Conference, Commission VI, WG VI/4, Beijing.
- Huang, C., Song, K., Kim, S., Townshend, J. R. G., Davis, P., Masek, J. G., & Goward, S. N. (2008). Use of a dark object concept and support vector machines to automate forest cover change analysis. *Remote Sensing of Environment*, *112*(3), 970-985.
- Im, J., & Jensen, J. R. J. R. S. o. E. (2005). A change detection model based on neighborhood correlation image analysis and decision tree classification. *99*(3), 326-340.
- Ingram, K., Knapp, E., & Robinson, J. J. N., Comput. Sci. Corp., Springfield, MD, CSC/TM-81/. (1981). Change detection technique development for improved urbanized area delineation.
- Jensen, J. R. J. M. o. R. S., second edition. (1983). Urban/suburban land use analysis. 1571-1666.
- Jin, S., & Sader, S. A. (2005). Comparison of time series tasseled cap wetness and the normalized difference moisture index in detecting forest disturbances. *Remote Sensing of Environment*, *94*(3), 364-372.
- Kemker, R., Salvaggio, C., & Kanan, C. (2018). Algorithms for semantic segmentation of multispectral remote sensing imagery using deep learning. *ISPRS Journal of Photogrammetry and Remote Sensing*, *145*, 60-77.
- Lillesand, T., Kiefer, R. W., & Chipman, J. (2015). *Remote sensing and image interpretation*: John Wiley & Sons.
- Liu, J., Chen, K., Xu, G., Sun, X., Yan, M., Diao, W., & Han, H. (2020). Convolutional Neural Network-Based Transfer Learning for Optical Aerial Images Change Detection. *IEEE Geoscience and Remote Sensing Letters*, *17*(1), 127-131.
- Liu, X., & Lathrop Jr, R. J. I. J. o. R. S. (2002). Urban change detection based on an artificial neural network. *23*(12), 2513-2518.

- Lu, D., Mausel, P., Brondizio, E., & Moran, E. J. I. j. o. r. s. (2004). Change detection techniques. *25*(12), 2365-2401.
- Martinez, J.-M., & Le Toan, T. (2007). Mapping of flood dynamics and spatial distribution of vegetation in the Amazon floodplain using multitemporal SAR data. *Remote sensing of environment*, *108*(3), 209-223.
- Martinis, S., Twele, A., & Voigt, S. (2011). Unsupervised Extraction of Flood-Induced Backscatter Changes in SAR Data Using Markov Image Modeling on Irregular Graphs. *IEEE transactions on geoscience and remote sensing*, *49*(1), 251-263.
- Miller, O., Pikaz, A., & Averbuch, A. (2005). Objects based change detection in a pair of gray-level images. *Pattern Recognition*, *38*(11), 1976-1992.
- Mishra, S., Shrivastava, P., & Dhurvey, P. (2017). Change detection techniques in remote sensing: A review. *International Journal of Wireless and Mobile communication for Industrial systems*, *4*(1), 1-8.
- Nelson, R. F. (1983). Detecting forest canopy change due to insect activity using Landsat MSS. *Photogrammetric Engineering Remote Sensing*, *49*(9), 1303-1314.
- Nemmour, H., & Chibani, Y. (2006a). Multiple support vector machines for land cover change detection: An application for mapping urban extensions. *ISPRS Journal of Photogrammetry and Remote Sensing*, *61*(2), 125-133.
- Nemmour, H., Chibani, Y. J. I. J. o. P., & Sensing, R. (2006b). Multiple support vector machines for land cover change detection: An application for mapping urban extensions. *61*(2), 125-133.
- Onur, I., Maktav, D., Sari, M., & Kemal Sönmez, N. (2009). Change detection of land cover and land use using remote sensing and GIS: a case study in Kemer, Turkey. *International Journal of Remote Sensing*, *30*(7), 1749-1757.
- Pijanowski, B. C., Pithadia, S., Shellito, B. A., & Alexandridis, K. J. I. J. o. G. I. S. (2005). Calibrating a neural network - based urban change model for two metropolitan areas of the Upper Midwest of the United States. *19*(2), 197-215.
- Qin, Y., Niu, Z., Chen, F., Li, B., & Ban, Y. (2013). Object-based land cover change detection for cross-sensor images. *International Journal of Remote Sensing*, *34*(19), 6723-6737.

- Quarmby, N. A., & Cushnie, J. L. (1989). Monitoring urban land cover changes at the urban fringe from SPOT HRV imagery in south-east England. *International Journal of Remote Sensing*, *10*(6), 953-963.
- Reid, R. S., Kruska, R. L., Muthui, N., Taye, A., Wotton, S., Wilson, C. J., & Mulatu, W. (2000). Land-use and land-cover dynamics in response to changes in climatic, biological and socio-political forces: the case of southwestern Ethiopia. *Landscape ecology*, *15*(4), 339-355.
- Richards, J. A. (1984). Thematic mapping from multitemporal image data using the principal components transformation. *Remote Sensing of Environment*, *16*(1), 35-46.
- Rogan, J., & Chen, D. (2004). Remote sensing technology for mapping and monitoring land-cover and land-use change. *Progress in planning*, *61*(4), 301-325.
- Rogerson, P. A. (2002). Change detection thresholds for remotely sensed images. *Journal of Geographical Systems*, *4*(1), 85-97.
- Schowengerdt, R. A. (2012). *Techniques for image processing and classifications in remote sensing*: Academic Press.
- Shi, W., Zhang, M., Zhang, R., Chen, S., & Zhan, Z. (2020). Change Detection Based on Artificial Intelligence: State-of-the-Art and Challenges. *Remote Sensing*, *12*(10). doi:10.3390/rs12101688
- Singh, A. (1989). Review Article Digital change detection techniques using remotely-sensed data. *International Journal of Remote Sensing*, *10*(6), 989-1003.
- Singh, A., & Harrison, A. (1985). Standardized principal components. *International Journal of Remote Sensing*, *6*(6), 883-896.
- Stow, D. (2010). Geographic object-based image change analysis. In *Handbook of applied spatial analysis* (pp. 565-582): Springer.
- Stow, D., DA, S., LR, T., & JE, E. (1980). Deriving land use/land cover change statistics from Landsat: a study of prime agricultural land.
- Strahler, A. H., Woodcock, C. E., & Smith, J. A. J. R. s. o. e. (1986). On the nature of models in remote sensing. *20*(2), 121-139.
- Swain, P. H. (1978). *Bayesian classification in a time-varying environment*. Retrieved from

- Taubenböck, H., Esch, T., Felbier, A., Wiesner, M., Roth, A., & Dech, S. (2012). Monitoring urbanization in mega cities from space. *Remote sensing of environment*, *117*, 162-176.
- Toll, D., Royal, J., & Davis, J. (1981). Urban area update procedures using Landsat data.
- Vapnik, V. N. (2000). *The nature of statistical learning theory* (2nd ed.. ed.). New York: New York : Springer-Verlag.
- Wang, X., Du, P., Liu, S., Senyshen, M., Zhang, W., Fang, H., & Fan, X. (2022). A novel multiple change detection approach based on tri-temporal logic-verified change vector analysis in posterior probability space. *International journal of applied earth observation and geoinformation*, *111*, 102852.
- Weismiller, R., Kristof, S., Scholz, D., Anuta, P., Momin, S. J. P. E., & Sensing, R. (1977). Change detection in coastal zone environments. *43*(12), 1533-1539.
- Wong, M. S., Zhu, X., Abbas, S., Kwok, C. Y. T., & Wang, M. (2021). Optical remote sensing. In *Urban informatics* (pp. 315-344): Springer.
- Woodcock, C. E., Macomber, S. A., Pax-Lenney, M., & Cohen, W. B. J. R. s. o. e. (2001). Monitoring large areas for forest change using Landsat: Generalization across space, time and Landsat sensors. *78*(1-2), 194-203.
- Xian, G., & Homer, C. (2010). Updating the 2001 National Land Cover Database Impervious Surface Products to 2006 using Landsat Imagery Change Detection Methods. *Remote Sensing of Environment*, *114*(8), 1676-1686.
- Yang, X., Zhang, K., Jia, B., & Ci, L. (2005). Desertification assessment in China: An overview. *Journal of arid environments*, *63*(2), 517-531.
- Yousif, O., & Ban, Y. (2013). Improving Urban Change Detection From Multitemporal SAR Images Using PCA-NLM. *IEEE transactions on geoscience and remote sensing*, *51*(4), 2032-2041.
- Yousif, O., & Ban, Y. (2015). *Object-based urban change detection using high resolution SAR images*. Paper presented at the 2015 Joint Urban Remote Sensing Event (JURSE).
- Yousif, O., Ban, Y. J. I. J. o. S. T. i. A. E. O., & Sensing, R. (2014). Improving SAR-based urban change detection by combining MAP-MRF classifier and nonlocal means similarity weights. *7*(10), 4288-4300.

- Zhang, C., Wei, S., Ji, S., & Lu, M. (2019). Detecting Large-Scale Urban Land Cover Changes from Very High Resolution Remote Sensing Images Using CNN-Based Classification. *ISPRS international journal of geo-information*, 8(4), 189.
- Zhang, C., Yue, P., Tapete, D., Jiang, L., Shangguan, B., Huang, L., & Liu, G. (2020). A deeply supervised image fusion network for change detection in high resolution bi-temporal remote sensing images. *ISPRS Journal of Photogrammetry and Remote Sensing*, 166, 183-200.
- Zhang, X., Xiao, P., Feng, X., & Yuan, M. (2017). Separate segmentation of multi-temporal high-resolution remote sensing images for object-based change detection in urban area. *Remote Sensing of Environment*, 201, 243-255.
- Zhao, W., Mou, L., Chen, J., Bo, Y., & Emery, W. J. (2020). Incorporating Metric Learning and Adversarial Network for Seasonal Invariant Change Detection. *IEEE Transactions on Geoscience and Remote Sensing*, 58(4), 2720-2731.
- Zhou, H., Zhang, M., Hu, X., Li, K., & Sun, J. (2021). A Siamese convolutional neural network with high–low level feature fusion for change detection in remotely sensed images. *Remote Sensing Letters*, 12(4), 387-396.
- Zhu, J., Su, Y., Guo, Q., & Harmon, T. C. (2017). Unsupervised object-based differencing for land-cover change detection. *Photogrammetric Engineering Remote Sensing*, 83(3), 225-236.